

# Autoignition of Methyl Valerate at Low to Intermediate Temperatures and Elevated Pressures in a Rapid Compression Machine

Bryan W. Weber<sup>a,\*</sup>, Justin Bunnell<sup>a</sup>, Kamal Kumar<sup>b</sup>, Chih-Jen Sung<sup>a</sup>

<sup>a</sup>*Department of Mechanical Engineering, University of Connecticut, Storrs, CT, USA*

<sup>b</sup>*Department of Mechanical Engineering, University of Idaho, Moscow, ID, USA*

---

## Abstract

Methyl valerate ( $\text{C}_6\text{H}_{12}\text{O}_2$ , methyl pentanoate) is a methyl ester and a relevant surrogate component for biodiesel. In this work, we present ignition delays of methyl valerate measured using a rapid compression machine at a range of engine-relevant temperature, pressure, and equivalence ratio conditions. The conditions we have studied include equivalence ratios from 0.25 to 2.0, temperatures between 680 K and 1050 K, and pressures of 15 bar and 30 bar. The ignition delay data demonstrate a negative temperature coefficient region in the temperature range of 720 K–800 K for both  $\phi = 2.0$ , 15 bar and  $\phi = 1.0$ , 30 bar, with two-stage ignition apparent over the narrower temperature ranges of 720 K–760 K for the lower pressure and 740 K–760 K at the higher pressure. In addition, the experimental ignition delay data are compared with simulations using an existing chemical kinetic model from the literature. The simulations with the literature model under-predict the data by factors between 2 and 10 over the entire range of the experimental data. To help determine the possible reasons for the discrepancy between simulations and experiments, a new chemical kinetic model is developed using the Reaction Mechanism Generator (RMG) software. The agreement between the experimental data and the RMG model is improved but still not satisfactory. Directions for future improvement of the methyl valerate model are discussed.

---

\*Corresponding Author: bryan.weber@uconn.edu

*Keywords:* chemical kinetics, rapid compression machine, autoignition, methyl ester

---

## 1. Introduction

For transportation applications, biodiesel is an important constituent in improving environmental friendliness of fuels, due to its renewability when produced from sustainable agricultural crops and its ability to reduce emissions relative to conventionally fueled engines [1]. A recent review paper summarizes the work on methyl esters relevant to biodiesel combustion [2]. Autoignition of methyl butanoate (MB,  $C_5H_{10}O_2$ ) has been well-studied in both shock tube and rapid compression machine experiments, and readers are referred to the review of [2] for further details. The prevalence of MB data in the literature is largely due to the early identification of MB as a potential surrogate fuel for biodiesel [3]. However, the experiments have shown that MB may not be an appropriate surrogate for biodiesel, due to its lack of negative temperature coefficient (NTC) behavior, a requirement for a suitable biodiesel surrogate [2].

Larger methyl esters such as methyl valerate (MV,  $C_6H_{12}O_2$ , methyl pentanoate) have also been studied as possible biodiesel surrogates. [4] used a rapid compression machine (RCM) to study the autoignition of several methyl esters including MV. Although MV exhibited two-stage ignition in this study, little additional research has been done on its oxidation. [5] studied MV in premixed laminar flames and extended a detailed high temperature chemical kinetic model to include MV and methyl hexanoate. [6] added MV to n-heptane/toluene fuel blends to determine the resulting intermediate species in premixed flames using a flat burner at 1 atm and an equivalence ratio of 1.75. The addition of MV helped reduce soot forming intermediates including benzene, cyclopentadienyl, acetylene, propargyl, and vinylacetylene [6]. [7] computationally examined the peroxy radical isomerization reactions for MV to better understand the low temperature reaction pathways. Finally, [8] used diffusion flames in the counter-flow configuration to determine extinction limits for a number of methyl esters,

including MV, and validated a detailed kinetic model with the experimental data.

This work provides additional data for the autoignition of MV. Data is collected in a RCM under engine relevant conditions spanning from 15 bar to 30 bar, equivalence ratios from 0.25 to 2.0, and temperatures from 682 K to 1048 K. The NTC region of MV is mapped out to provide additional information on the fidelity of using MV as a biodiesel surrogate.

## 2. Experimental Methods

The RCM used in this study is a single piston arrangement and is pneumatically driven and hydraulically stopped. The device has been described in detail previously [9] and will be described here briefly for reference. The end of compression (EOC) temperature and pressure ( $T_C$  and  $P_C$  respectively), are independently changed by varying the overall compression ratio, initial pressure ( $P_0$ ), and initial temperature ( $T_0$ ) of the experiments. The primary diagnostic on the RCM is the in-cylinder pressure. The pressure data is processed by a Python package called UConnRCMPy [10], which calculates  $P_C$ ,  $T_C$ , and the ignition delay(s). The definitions of the ignition delays are shown in Fig. 1. The time of the EOC is defined as the maximum of the pressure trace prior to the start of ignition and the ignition delays are defined as the time from the EOC until local maxima in the first time derivative of the pressure. Each experimental condition is repeated at least five times to ensure repeatability of the data. As there is some random scatter present in the data, the standard deviation ( $\sigma$ ) of the ignition delays from the runs at a given condition is computed. In all cases,  $\sigma$  is less than 10 % of the mean value of the overall ignition delay.

In addition to the reactive experiments, non-reactive experiments are conducted to determine the influence of machine-specific behavior on the experimental conditions and permit the calculation of the EOC temperature via the isentropic relations between pressure and temperature [11]. The EOC temperature is calculated by the procedure described in Section 3.

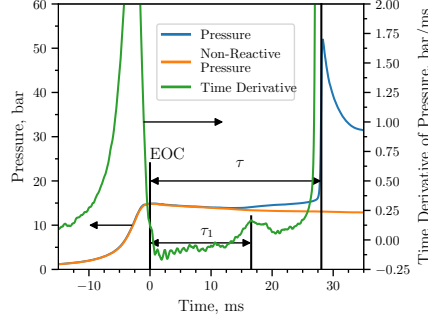


Figure 1: Definition of the ignition delays used in this work. The experiment in this figure was conducted for a  $\phi = 2.0$  mixture with  $\text{Ar}/(\text{N}_2 + \text{Ar}) = 0.5$ ,  $P_0 = 0.7694$  bar,  $T_0 = 373$  K,  $P_C = 14.94$  bar,  $T_C = 723$  K,  $\tau = (27.44 \pm 0.99)$  ms,  $\tau_1 = (16.57 \pm 0.48)$  ms.

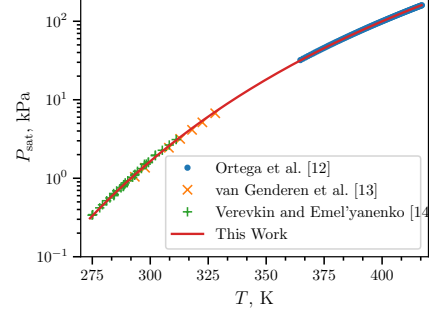


Figure 2: Saturated vapor pressure of MV as a function of temperature, plotted using the Antoine equation, Eq. (1), with  $A = 6.4030$ ,  $B = 1528.69$ , and  $C = 52.881$ .

57 The RCM is equipped with heaters to control the initial temperature of the  
 58 mixture. After filling in the components to the mixing tanks, the heaters are  
 59 switched on and the system is allowed 1.5 h to come to steady state. The mixing  
 60 tanks are also equipped with magnetic stir bars so the reactants are well mixed  
 61 for the duration of the experiments.

The initial temperature is chosen such that the saturated vapor pressure ( $P_{\text{sat}}$ ) of the fuel at the initial temperature is at least twice the partial pressure of the fuel in the mixing tank. The Antoine equation

$$\log_{10} P_{\text{sat}} = A - \frac{B}{T - C} \quad (1)$$

62 is used to model the saturated vapor pressure of MV as a function of tempera-  
 63 ture, where  $A$ ,  $B$ , and  $C$  are substance-specific coefficients. The coefficients in  
 64 Eq. (1) are determined by least squares fitting of the data of [12], [13], and [14]  
 65 using the `curve_fit()` function of SciPy [15] version 0.18.1. Figure 2 shows  
 66 that the coefficients fit with this procedure give good agreement with the ex-  
 67 perimental data.

68 The mixtures considered in this study are shown in Table 1. Mixtures are

69 prepared in stainless steel mixing tanks. The proportions of reactants in the  
70 mixture are determined by specifying the absolute mass of the fuel, the equiv-  
71 alence ratio ( $\phi$ ), and the ratio of Ar : N<sub>2</sub> in the oxidizer. Since MV is a liquid  
72 with a relatively small vapor pressure at room temperature, it is injected into  
73 the mixing tank through a septum. Proportions of O<sub>2</sub>, Ar, and N<sub>2</sub> are added  
74 manometrically at room temperature.

Table 1: Mixtures considered in this work

$\phi$	Mole Fraction (purity)				Ar/(N <sub>2</sub> + Ar)
	MV (100 %)	O <sub>2</sub> (99.994 %)	Ar (99.999 %)	N <sub>2</sub> (99.999 %)	
0.25	0.0065	0.2087	0.7848	0.0000	1.0
0.5	0.0130	0.2074	0.7798	0.0000	1.0
1.0	0.0256	0.2047	0.7697	0.0000	1.0
1.0	0.0256	0.2047	0.3849	0.3848	0.5
2.0	0.0499	0.1996	0.0000	0.7505	0.0
2.0	0.0499	0.1996	0.3752	0.3753	0.5

### 75 3. Computational Methods

#### 76 3.1. RCM Modeling

77 The Python 3.5 interface of Cantera [16] version 2.2.1 is used for all sim-  
78 ulations in this work. Detailed descriptions of the use of Cantera for these  
79 simulations can be found in the work of [17] and [18]; a brief overview is given  
80 here. As mentioned in Section 2, non-reactive experiments are conducted to  
81 characterize the machine-specific effects on the experimental conditions in the  
82 RCM. This pressure trace is used to compute a volume trace by assuming that  
83 the reactants undergo a reversible, adiabatic, constant composition (i.e., isen-  
84 tropic) compression during the compression stroke and an isentropic expansion  
85 after the EOC. The volume trace is applied to a simulation conducted in an

86 `IdealGasReactor` in Cantera [16] using the CVODES solver from the SUNDI-  
 87 ALS suite [19]. The ignition delay from the simulations is defined in the same  
 88 manner as in the experiments. The time derivative of the pressure in the sim-  
 89 ulations is computed by second order Lagrange polynomials, as discussed by  
 90 [20].

91 To the best of our knowledge, there are three mechanisms for MV combustion  
 92 available in the literature. The first two, by [5] and [6], were developed to  
 93 simulate flames, and do not include the low-temperature chemistry necessary to  
 94 simulate the conditions in these experiments. The third model was developed  
 95 by [8] and includes low-temperature chemistry of MV, although it was only  
 96 validated by comparison with flame extinction limits. The detailed [8] model  
 97 includes 1103 species and 7557 reactions.

### 98 *3.2. Reaction Mechanism Generator*

99 In addition to using a mechanism from the literature, we investigate the use  
 100 of an automatic mechanism generator, the open-source Reaction Mechanism  
 101 Generator (RMG) [21] version 1.0.4. The Python version of RMG is used, which  
 102 requires Python 2.7, and version 1.10.0 of the RMG database is used. The final  
 103 RMG model contains 483 species and 19990 reactions. Note that the number  
 104 of species is much lower than the [8] model because the RMG model focuses on  
 105 only one fuel (MV), but the number of reactions is substantially higher.

## 106 **4. Experimental Results**

107 Figure 3 shows the ignition delay results measured in this study. Filled mark-  
 108 ers denote the overall ignition delay and hollow markers indicate the first-stage  
 109 ignition delay. Vertical error bars are drawn on the symbols to represent the  
 110 uncertainty in the ignition delay; for many of the experiments, the uncertainty  
 111 is approximately the same size as the data point, so the error bar is hidden.  
 112 Horizontal error bars are shown on the first and last points of each equivalence  
 113 ratio indicating the estimated uncertainty in the EOC temperature of  $\pm 1\%$  [22].

Fig. 3a shows the results for a compressed pressure of 15 bar, while Fig. 3b shows the results for a compressed pressure of 30 bar. Note that  $\phi = 2.0$  results were not collected for 30 bar, so there are no red data points in Fig. 3b.

It can be seen from Fig. 3 that the ignition delays for the  $\phi = 0.25$  and 0.5 mixtures do not show an NTC region of the ignition delay for both of the pressures studied in this work. However, the  $\phi = 1.0$  mixture shows an NTC region at  $P_C = 30$  bar between approximately 720 K and 800 K, with measured first-stage ignition delays at 734 K and 757 K. In addition, the  $\phi = 2.0$  mixture shows an NTC region of ignition delay at 15 bar from approximately 720 K to 775 K, with measured first-stage ignition delays between 720 K and 750 K.

Figure 4 shows the pressure traces for selected experiments at  $\phi = 1.0$ ,  $P_C = 30$  bar. The three reactive pressure traces shown are at the low-temperature end of the NTC (blue, 700 K), one case with two-stage ignition (orange, 734 K), and one case near the high-temperature limit of the NTC region (green, 775 K). Also shown is the non-reactive pressure trace for the 700 K case (red). By comparing the 700 K pressure trace with the non-reactive pressure trace, it can be seen that there is substantial heat release prior to main ignition as measured by the deviation of the reactive pressure trace from the non-reactive trace. However, there is only one peak in the time derivative of the pressure, so no first-stage ignition delay is defined for this case. It can also be seen in Fig. 4 that the 775 K case shows some heat release prior to ignition, although again there is only one peak in the time derivative of the pressure. Furthermore, the heat release at 775 K appears to be more gradual than at the lowest temperature.

## 5. Computational Results

Figure 5 compares experimentally measured overall ignition delays with ignition delays computed with the detailed model of [8] for the  $\phi = 1.0$  experiments. Results for the other equivalence ratios are similar to these results, so are not shown here. It is important to note that the model of [8] was not validated for MV ignition delays, only for extinction strain rates. At 15 bar, the model

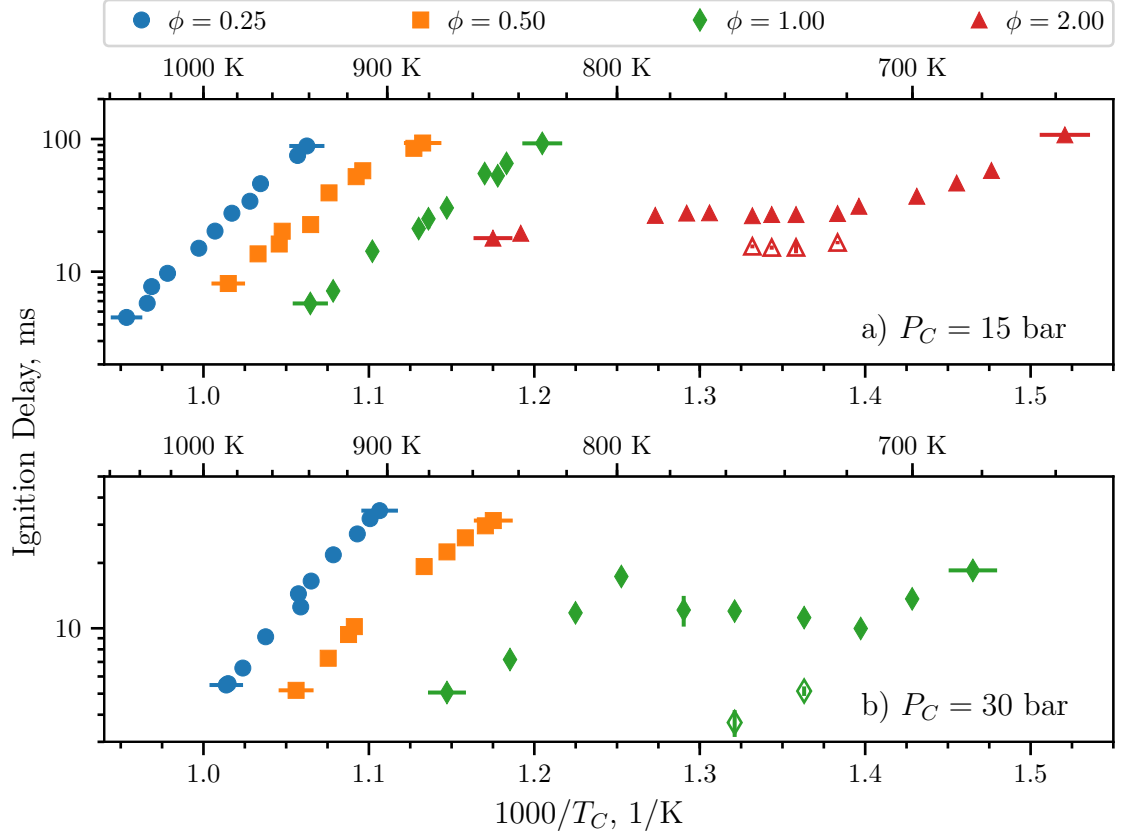


Figure 3: Ignition delays of MV as a function of inverse temperature. Filled points are the overall ignition delays and hollow points are the first stage ignition delays. a) 15 bar. b) 30 bar

143 tends to under-predict the ignition delay and predicts an NTC region that is not  
 144 present in the experiments. At 30 bar, the model predicts the low-temperature  
 145 ignition delays well, but does not predict the NTC region found experimentally.

146 To understand the underlying reasons for the disagreement between the [8]  
 147 model and the data, we constructed an additional model using RMG (see Sec-  
 148 tion 3.2). As can be seen in Fig. 5, the agreement between the RMG model and  
 149 the experimental data is similar to the [8] model for the 30 bar data. At 15 bar,  
 150 the RMG model predicts a somewhat longer ignition delay than the model of  
 151 [8], but still predicts an NTC region where none is present in the experimental



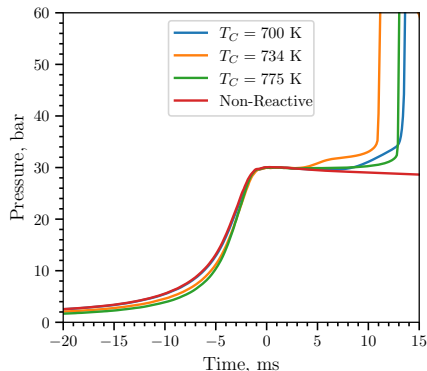


Figure 4: Selected pressure traces around the NTC region of ignition delay for  $\phi = 1.0$

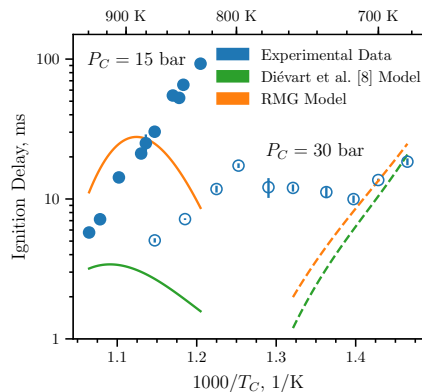


Figure 5: Comparison of experimental and simulated results for  $\phi = 1.0$

data.

In general, there could be three likely sources of error in the models: missing reaction pathways, incorrect values of the reaction rates, and incorrect values for thermodynamic properties of the species. We have noted in Section 3.2 that the RMG model has many more reactions than the [8] model and the algorithm used in RMG considers a substantial number of the possible pathways. This reduces the possibility of missing reaction pathways affecting the model. Further detailed studies are required to ensure that the RMG model includes all of the relevant reaction pathways.

The second source of error may be incorrect reaction rate parameters, either because the rates are specified incorrectly in the model (e.g., typos) or because the rates are not well estimated by the typical analogy based-rules. It should be noted that errors of this type may affect the model generated by RMG—if the rates are not estimated correctly, reactions that are important in reality may not be included in the model. Determining the accuracy of the reaction rates used in the RMG and [8] models requires further detailed studies of the models. Another related source of error could be incorrect estimation of the pressure dependence of the reaction rates, which may be particularly important for the isomerization reactions prevalent in low-temperature chemistry.

171 The third source of error may lie in the estimation of the thermodynamic  
 172 properties of the species, particularly their heats of formation. We have begun to  
 173 analyze the possibility of this source of error by conducting a reaction pathway  
 174 analysis to determine which radicals are formed from the breakdown of the fuel.  
 175 The following analysis is conducted for a constant volume simulation at 700 K,  
 176 30 bar, where the rates of production of the species have been integrated until  
 177 the time of 20 % fuel consumption. The results of this analysis are shown in  
 178 Fig. 6 and Table 2 for the two models. The percentages shown in the Table 2  
 179 are the percent of the fuel destroyed to form a particular fuel radical by all the  
 180 reactions that can form that radical.

181 At the relatively low temperature and high pressure condition of this analy-  
 182 sis, all of the fuel is destroyed by H-atom abstractions to form the fuel radicals  
 183 shown. It can be seen that the two models have quite different distributions of  
 184 products from the first H-abstraction reactions. The model of [8] predicts that  
 185 H-abstraction from the second carbon is the most prevalent, followed closely by  
 186 abstraction from the methyl group. This is in line with the bond energies of the  
 187 C-H bonds for those carbon atoms; we expect that the presence of the oxy-  
 188 gen atoms will cause hydrogen abstraction at the nearby carbons to be favored.  
 189 However, the RMG model predicts that radicals in the middle of the carbon  
 190 chain will be primarily formed. The cause of this discrepancy is under investi-  
 191 gation, but it may be caused by the estimation of thermodynamic properties of  
 192 the radicals.

## 193 **6. Conclusions**

194 In this study, we have measured ignition delays for methyl valerate over a  
 195 wide range of engine-relevant pressures, temperatures, and equivalence ratios.  
 196 An NTC region of the ignition delay and two-stage ignition were recorded for  
 197 pressures of 15 bar at  $\phi = 2.0$  and 30 bar at  $\phi = 1.0$ . A detailed chemical ki-  
 198 netic model available in the literature was unable to reproduce the experimental  
 199 results, so a new model was constructed using the Reaction Mechanism Gen-

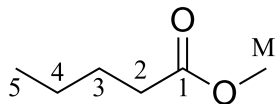


Figure 6: Structure of MV with carbon atoms labeled according to the convention used in Table 2

Table 2: Percent of MV destroyed to form fuel radical species with a hydrogen atom missing at the location indicated in the first column

Radical Site	[8] [%]	RMG Model [%]
2	29.3	7.4
3	17.5	36.0
4	17.5	41.1
5	9.4	3.7
M	26.3	11.8

erator software. Although the new model contains many more reactions than the literature model, it is still unable to predict the experimental ignition delays satisfactorily. Possible reasons for the discrepancy include missing reaction pathways, incorrect rate estimates, and incorrect thermodynamic property estimates. Future work will include investigation of the discrepancies between models and experiments to further understand the autoignition kinetics of methyl valerate.

## References

- [1] S. K. Hoekman, C. Robbins, Review of the effects of biodiesel on NO<sub>x</sub> emissions 96 237–249. doi:10.1016/j.fuproc.2011.12.036.
- [2] L. Coniglio, H. Bennadji, P. Glaude, O. Herbinet, F. Billaud, Combustion chemical kinetics of biodiesel and related compounds (methyl and ethyl esters): Experiments and modeling Advances and future refinements 39 (4) 340–382. doi:10.1016/j.pecs.2013.03.002.
- [3] E. Fisher, W. J. Pitz, H. J. Curran, C. K. Westbrook, Detailed chemical kinetic mechanisms for combustion of oxygenated fuels 28 (2) 1579–1586, 10. doi:10.1016/S0082-0784(00)80555-X.

- [4] K. Hadj-Ali, M. Crochet, G. Vanhove, M. Ribaucour, R. Minetti, A study of the low temperature autoignition of methyl esters 32 (1) 239–246, 23. doi:10.1016/j.proci.2008.09.002.
- [5] O. P. Korobeinichev, I. E. Gerasimov, D. A. Knyazkov, A. G. Shmakov, T. A. Bolshova, N. Hansen, C. K. Westbrook, G. Dayma, B. Yang, An Experimental and Kinetic Modeling Study of Premixed Laminar Flames of Methyl Pentanoate and Methyl Hexanoate 229 (5). doi:10.1515/zpch-2014-0596.
- [6] A. M. Dmitriev, D. A. Knyazkov, T. A. Bolshova, A. G. Shmakov, O. P. Korobeinichev, The effect of methyl pentanoate addition on the structure of premixed fuel-rich n-heptane/toluene flame at atmospheric pressure 162 (5) 1964–1975. doi:10.1016/j.combustflame.2014.12.015.
- [7] C. Hayes, D. R. Burgess, Exploring the oxidative decompositions of methyl esters: Methyl butanoate and methyl pentanoate as model compounds for biodiesel 32 (1) 263–270, 26. doi:10.1016/j.proci.2008.05.075.
- [8] P. Divart, S. H. Won, J. Gong, S. Dooley, Y. Ju, A comparative study of the chemical kinetic characteristics of small methyl esters in diffusion flame extinction 34 (1) 821–829. doi:10.1016/j.proci.2012.06.180.
- [9] G. Mittal, C.-J. Sung, A Rapid Compression Machine for Chemical Kinetics Studies at Elevated Pressures and Temperatures 179 (3) 497–530. doi:10.1080/00102200600671898.
- [10] B. W. Weber, C.-J. Sung, UConnRCMPy.  
URL <https://github.com/bryanweber/UConnRCMPy/releases/tag/v2.1.0>
- [11] D. Lee, S. Hochgreb, Rapid Compression Machines: Heat Transfer and Suppression of Corner Vortex 114 531–545. doi:10.1016/S0010-2180(97)00327-1.

- [12] J. Ortega, F. Espiau, J. Tojo, J. Canosa, A. Rodriguez, Isobaric VaporLiquid Equilibria and Excess Properties for the Binary Systems of Methyl Esters + Heptane 48 (5) 1183–1190. doi:10.1021/je030117d.
- [13] A. C. van Genderen, J. van Miltenburg, J. G. Blok, M. J. van Bommel, P. J. van Ekeren, G. J. van den Berg, H. A. Oonk, Liquidvapour equilibria of the methyl esters of alkanolic acids: Vapour pressures as a function of temperature and standard thermodynamic function changes 202 (1) 109–120. doi:10.1016/S0378-3812(02)00097-3.
- [14] S. P. Verevkin, V. N. Emelyanenko, Transpiration method: Vapor pressures and enthalpies of vaporization of some low-boiling esters 266 64–75. doi:10.1016/j.fluid.2008.02.001.
- [15] E. Jones, T. Oliphant, P. Peterson, others, SciPy: Open Source Scientific Tools for Python.  
URL <http://www.scipy.org/>
- [16] D. G. Goodwin, H. K. Moffat, R. L. Speth, Cantera: An Object-oriented Software Toolkit for Chemical Kinetics, Thermodynamics, and Transport Processes.  
URL <http://www.cantera.org>
- [17] B. W. Weber, C.-J. Sung, UConnRCMPy: Python-based Data Analysis for Rapid Compression Machines, in: S. Benthall, S. Rostrup (Eds.), Proceedings of the 15th Python in Science Conference, pp. 36–44.
- [18] E. E. Dames, A. S. Rosen, B. W. Weber, C. W. Gao, C.-J. Sung, W. H. Green, A detailed combined experimental and theoretical study on dimethyl ether/propane blended oxidation 168 310–330. doi:10.1016/j.combustflame.2016.02.021.
- [19] A. C. Hindmarsh, P. N. Brown, K. E. Grant, S. L. Lee, R. Serban, D. E. Shumaker, C. S. Woodward, SUNDIALS: Suite of

- 270 nonlinear and differential/algebraic equation solvers 31 (3) 363–396.  
271 doi:10.1145/1089014.1089020.
- 272 [20] S. C. Chapra, R. P. Canale, Numerical Methods for Engineers, 6th Edition,  
273 McGraw-Hill Higher Education.
- 274 [21] J. W. Allen, C. F. Goldsmith, W. H. Green, Automatic estimation of  
275 pressure-dependent rate coefficients. 14 (3) 1131–1155, bibtex: Allen2012.  
276 doi:10.1039/c1cp22765c.  
277 URL <http://xlink.rsc.org/?DOI=C1CP22765C>
- 278 [22] B. W. Weber, C.-J. Sung, M. W. Renfro, On the uncertainty of tem-  
279 perature estimation in a rapid compression machine 162 (6) 2518–2528.  
280 doi:10.1016/j.combustflame.2015.03.001.